Fibrotic Encapsulation Is the Dominant Source of Continuous Glucose Monitor Delays

P. Mason McClatchey,[1] Ethan S. McClain,[2] Ian M. Williams,[1] Carlo M. Malabanan,[3] Freyja D. James,[1] Peter C. Lord,[4] Justin M. Gregory,[5] David E. Cliffel,[2] and David H. Wasserman[1,3]

Diabetes 2019;68:1892–1901 | https://doi.org/10.2337/db19-0229

TECHNOLOGICAL ADVANCES

Continuous glucose monitor (CGM) readings are delayed relative to blood glucose, and this delay is usually attributed to the latency of interstitial glucose levels. However, CGM-independent data suggest rapid equilibration of interstitial glucose. This study sought to determine the loci of CGM delays. Electrical current was measured directly from CGM electrodes to define sensor kinetics in the absence of smoothing algorithms. CGMs were implanted in mice, and sensor versus blood glucose responses were measured after an intravenous glucose challenge. Dispersion of a fluorescent glucose analog (2-NBDG) into the CGM microenvironment was observed in vivo using intravital microscopy. Tissue deposited on the sensor and nonimplanted subcutaneous adipose tissue was then collected for histological analysis. The time to half-maximum CGM response in vitro was 35 ± 2 s. In vivo, CGMs took 24 ± 7 min to reach maximum current versus 2 ± 1 min to maximum blood glucose (P = 0.0017). 2-NBDG took 21 ± 7 min to reach maximum fluorescence at the sensor versus 6 ± 6 min in adipose tissue (P = 0.0011). Collagen content was closely correlated with 2-NBDG latency (R = 0.96, P = 0.0004). Diffusion of glucose into the tissue deposited on a CGM is substantially delayed relative to interstitial fluid. A CGM that resists fibrous encapsulation would better approximate real-time deviations in blood glucose.

Continuous glucose monitor (CGM) readings can lag behind blood glucose by as much as 20 min, and this delay limits their use as a stand-alone glucose-monitoring technology (1). In laboratory settings, glucose oxidase sensors can record fluctuations in glucose concentration with millisecond-scale time resolution (2), thus raising the question of why CGM readings are so delayed. Substantial efforts have been made to identify the sources of CGM latency using an indirect approach (3). By subtracting known sources of delay from the observed total, these analyses have generally concluded that the physiological latency of interstitial glucose concentration is a major contributor to CGM delays and that the remainder of the delay is largely caused by CGM smoothing algorithms. A significant role for interstitial glucose latency is further supported by microdialysis and lymphatic measurements indicating a significant delay between blood and interstitial glucose concentrations (4,5). Because of these findings, interstitial glucose latency as a limitation in CGM technology has generally been taken for granted.

However, claims of a sizable delay in the equilibration of glucose between blood and interstitial fluid contrast markedly with data from integrative physiology studies suggesting rapid glucose dispersion into the interstitium (6–8). Glucose exhibits a sizable arteriovenous concentration difference (7), and capillary transit time is on the order of 1–3 s (9). These data suggest blood and interstitial glucose must equilibrate within seconds. Furthermore, direct measurements of glucose diffusion in human tissues suggest an in vivo diffusion rate of >100 $\mu m^2/s$ (8), whereas capillary densities in human adipose tissue and muscle are generally on the order of ~200–300 capillaries/mm^2 (10,11), corresponding to a diffusion radius of ~70 μm. Analysis from first principles therefore further supports the notion of glucose equilibration on the order of seconds rather than minutes. Such incongruities in estimates of time required for glucose efflux from capillaries do not necessarily stem from methodological

[1]Department of Molecular Physiology and Biophysics, Vanderbilt University, Nashville, TN
[2]Department of Chemistry, Vanderbilt University, Nashville, TN
[3]Mouse Metabolic Phenotyping Center, Vanderbilt University, Nashville, TN
[4]PhysioLogic Devices, Inc., Alpine, CA
[5]Ian M. Burr Division of Pediatric Endocrinology and Diabetes, Vanderbilt University School of Medicine, Nashville, TN

Corresponding author: P. Mason McClatchey, pmasonmcclatchey@gmail.com

Received 4 March 2019 and accepted 17 July 2019

differences. Interstitial glucose delays inferred from lymphatic measurements range from nearly immediate to >5 min (5,6) despite similar data and superficially similar analysis assumptions.

An additional parameter that may reconcile results in CGM studies with those in integrative physiology contexts is that CGMs experience a robust foreign body response (12,13). This effect is most often discussed as a functional limitation for long-term implantation of CGMs. However, fibrosis and gene expression profiles consistent with hypoxia are observed within 3 days of sensor implantation (14), suggesting that the dispersion of oxygen and nutrients into the CGM microenvironment is impaired within days. Much of the research concerning the effects of the foreign body response on CGM accuracy has focused on cellular and biochemical effects that interfere with detection of glucose by glucose oxidase (15–17). However, foreign body capsules have been shown to slow the diffusion of interstitial solutes (18), and this effect has been postulated to delay the arrival of glucose in the CGM microenvironment (19). That said, the magnitude and functional importance of this effect within the time frames characteristic of commercial CGM usage are currently unknown, and the high rate of glucose diffusion observed in vivo may render foreign body response–induced delays negligible relative to those caused by smoothing algorithms and genuine interstitial latency, among others. Furthermore, it is unclear whether putative delays caused by fibrous encapsulation of the sensor could take effect early enough after implantation to meaningfully influence results with contemporary CGMs, which are typically implanted for no more than 2 weeks.

This study addresses the hypothesis that glucose fluctuations in the CGM microenvironment are delayed relative to blood glucose primarily as a result of fibrous encapsulation of the implanted sensor. To isolate delays in glucose exposure from delays caused by smoothing algorithms, we disassembled the sensor and took readings directly from the electrodes every second both in vivo and in vitro. To determine whether in vivo responses were delayed due to genuine delays in local glucose concentrations as opposed to other unknown interactions between the sensor and tissue, we used a fluorescent glucose analog (2-NBDG) (20) to directly visualize the dispersion of glucose using intravital fluorescence microscopy. 2-NBDG kinetics were then compared between the sensor microenvironment, nonimplanted subcutaneous adipose tissue, and skeletal muscle to define the excess delay in the sensor microenvironment. Collectively, these experiments seek to provide a comprehensive framework describing the delivery of glucose to the membrane of an implanted CGM. This information will identify sources of latency and the barriers necessary to make the use of CGM as a stand-alone system for glucose monitoring in patients with diabetes by identifying the causes of inaccuracies and latency of CGM readings.

RESEARCH DESIGN AND METHODS

Sensors

Dexcom G4 CGMs were used for this study. The Dexcom G4 transmitter provides one reading every 5 min, whereas the hypotheses of this study required sampling on the order of seconds. Therefore, sensors were disassembled to expose their working and reference electrodes (Fig. 1), which were connected to the leads of a CHI 1440 potentiostat (CH Instruments) to provide 1 Hz measurements of sensor current. The Dexcom G4 is designed for 7 days of use but is often used for up to 14 days (21). Therefore, in vivo experiments were performed 7–13 days after sensor implantation to reflect clinically relevant conditions.

Animals

The study used C57Bl/J6 wild-type male mice at 8 weeks of age. Mice (n = 10 mice) were implanted with indwelling jugular vein catheters 1 week before in vivo sensor testing (22). CGMs were implanted after blunt dissection of the dorsal subcutaneous space as part of the catheterization surgery. Mice were then returned to the colony for 1 week, at which time they were weighed to ensure recovery to within 10% original body weight. Sensor and blood glucose responses to an intravenous glucose challenge (1 g/kg) were then recorded. Finally, mice underwent intravital microscopy experiments 13 days after CGM implantation to visualize the dispersion of a fluorescent glucose analog, 2-NBDG (20), in the sensor microenvironment and adjacent non–CGM-implanted subcutaneous adipose tissue. An additional eight mice underwent similar intravital microscopy experiments to visualize 2-NBDG dispersion in skeletal muscle. Mice were sacrificed by cervical dislocation after intravital microscopy, and tissues were collected for histological analysis. All procedures were performed under isoflurane anesthesia. The Vanderbilt University Animal Care and Use Committee approved the experiments.

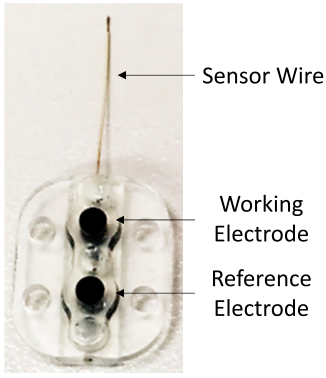

Figure 1—Illustration of disassembled glucose sensor. Sensors were disassembled to expose the sensor electrodes for unprocessed readings of sensor current. The Dexcom G4 uses a two-electrode configuration with working and reference electrodes, as indicated in the above illustration.

In Vitro Sensor Testing

To determine the intrinsic kinetics and signal quality of the sensor, four disassembled CGMs were tested in vitro. First, the baseline sensor current was defined by being incubated in 2 mmol/L PBS with 120 mmol/L KCl for 5 min. The sensor was then successively moved to solutions containing increasing concentrations from 5 to 25 mmol/L glucose in increments of 5 mmol/L. An incubation time of 5 min was used for each concentration to allow sensor current to reach steady state. The potentiostat was held at 0.6 V versus reference, and current values were recorded at 1 Hz for the duration of the experiment.

The average current in the last 30 s at each glucose concentration was used to create a dose-response curve for each sensor. The approach from one steady-state value to the next was fit to a single exponential decay to calculate the rate of sensor response using the natural log of current to linearize the transient portion of the curve, as shown in Eqs. 1–3, thus yielding six independent kinetics measurements (one per solution tested) per sensor. Because the time to half-maximum (T_{50}) current proved to be highly consistent within each sensor (±5 s) and did not vary with glucose concentration, measurements were averaged to yield a value for each sensor.

$$y = e^{-k*T} \quad [1]$$

$$0.5 = e^{-k*T_{50}} \quad \rightarrow \quad \ln(0.5) = -k*T_{50} \quad [2]$$

$$T_{50} = -\frac{k}{\ln(0.5)} \quad [3]$$

In Vivo Sensor Testing

After sensor kinetics in vitro were determined, CGM response was compared with the blood glucose response after an intravenous glucose challenge in vivo. Mice were fasted for 5 h and then anesthetized using isoflurane (dose of 2% at 200 mL/min for induction, 1.5% at 80 mL/min for maintenance) to mitigate mechanical disturbances of the sensor or potentiostat leads. Sensor current was recorded every 5 min until it stabilized for at least 15 min. Subsequently, mice received intravenous infusions of 1 g/kg dextrose (Hospira). Tail blood glucose was tested every minute for the first 10 min after the injection and then every 5 min until 30 min after the injection. Meanwhile, sensor current was recorded at 1 Hz throughout the entire 30-min time course. The average sensor current in the 30 s before each blood glucose sample was used to obtain CGM values time matched to blood glucose measurements. Because sensor current was subject to major, unpredictable deviations in vivo, the median was used to define the 30 s average rather than the mean to mitigate the influence of individual outliers.

Intravital Microscopy

Intravital microscopy experiments were performed in fasted mice 6 days after in vivo sensor response testing (day 13 after CGM insertion) to observe the dispersion of a fluorescent glucose analog, 2-NBDG (20), into the sensor microenvironment and non–CGM-implanted subcutaneous adipose tissue, which was used for comparison. Mice were anesthetized using isoflurane, as described in the previous section, and the skin above the implanted sensor was trimmed away to expose the sensor and surrounding subcutaneous adipose tissue. Exposed tissue was placed flush against a glass coverslip immersed in isotonic saline, similar to our previously published techniques for skeletal muscle visualization (22,23). Body temperature was maintained at 37°C using an infrared heating blanket and temperature probe (Kent Scientific). Mice were equilibrated on the microscope stage for 15 min before imaging to ensure a stable physiological baseline.

Visualization of 2-NBDG dispersion was performed using a spinning disc microscope (Nikon Instruments) equipped with a Yokogawa CSU-X1 spinning disk head, an Andor DU-897 electron multiplying charge-coupled device (EMCCD) camera, and a Plan Apochromat Lambda 20× objective (0.75 numerical aperture, 0.65 μm pixel size). A 488-nm (16.25-mW) laser diode with 70 ms exposure time was used to excite 2-NBDG fluorescence. Images were captured at 4.72 frames/s for the first 45 s after intravenous 2-NBDG injection to provide high time resolution for initial influx of 2-NBDG, after which images were captured at 1 frame/s for an additional 30 min. This procedure was performed sequentially at the sensor and in adjacent, nonimplanted subcutaneous adipose tissue for each mouse. The order of acquisition (i.e., adipose first vs. sensor first) was randomized to prevent confounding effects of differing time under anesthesia, residual 2-NBDG fluorescence, etc. A dose of 2.5 μg 2-NBDG in 50 μL saline was used for each acquisition, yielding a total of 5 μg 2-NBDG with 100 μL injection volume.

Whole field of view 2-NBDG fluorescence was normalized within each time series to a starting value of 0 and a maximum of 1, and the T_{50} and time to maximum 2-NBDG fluorescence were recorded. In addition to sensor and subcutaneous adipose tissue images, 2-NBDG dispersion in skeletal muscle was visualized in a separate cohort of mice ($n = 8$) to provide values for comparison of interstitial latency in muscle versus subcutaneous adipose tissue.

Histological Analysis

Upon dissection, sensors were noted to be coated in fibrous deposits. The sensor wire was cut free from the electrode housing and dissected out with deposited tissue intact. Sensor deposits, along with adjacent non–CGM-implanted subcutaneous adipose tissue, were fixed in formalin. All samples were subsequently sent to the Vanderbilt Translational Pathology Shared Resource, where they were embedded in paraffin, cut into 5-μm sections, and stained with hematoxylin-eosin and Masson trichrome. Stained sections then underwent whole-slide imaging in the Vanderbilt Digital Histology Shared Resource. Collagen content was assessed by fraction of total tissue stained positive for Masson trichrome as detected using Leica Biosystems.

Statistics

All statistics were performed using GraphPad Prism software (GraphPad Software). Comparisons within the same mouse were performed using paired t tests, and comparisons between mice were performed using unpaired t tests. Departure from a normal distribution was assessed for each variable using the D'Agostino and Pearson omnibus normality test. No distributions were found to be significantly nonnormal (all P = NS). Correlations were assessed using Pearson R, and goodness of fit was assessed using R^2. Statistical significance is reported using precise P values unless $P < 0.0001$. Data are presented as mean ± SD unless otherwise noted.

RESULTS

In Vitro Sensor Testing

In vitro sensor testing results are shown in Fig. 2. Sensor current rapidly changed in response to glucose concentration (Fig. 2*A*). Current amplitude increased (i.e., became more negative) with increasing glucose concentration. Large deviations in electrical signal resulting from handling of the sensor (visible as spikes between successive glucose concentrations in Fig. 2*A*) were excluded from analysis and were observed to be large relative to intrinsic instrument noise. Steady-state current was linear with respect to glucose concentration (Fig. 2*B*). The equilibration of sensor current upon transitioning from one glucose concentration to the next was well described by a single-exponential fit (Fig. 2*C*). Compiled results are shown in Fig. 2*D*. Individual sensors were highly variable in their sensitivity to glucose, with maximum steady-state currents ranging over an order of magnitude. However, all sensors showed a linear relationship to glucose concentration ($R^2 \geq 0.97$), and all had a T_{50} within 3 s of 35 s (time constant ~50 s), indicating substantial consistency in sensor accuracy and kinetics.

In Vivo Sensor Testing

Results from in vivo sensor testing are summarized in Fig. 3. The raw CGM signal in vivo exhibited substantial noise,

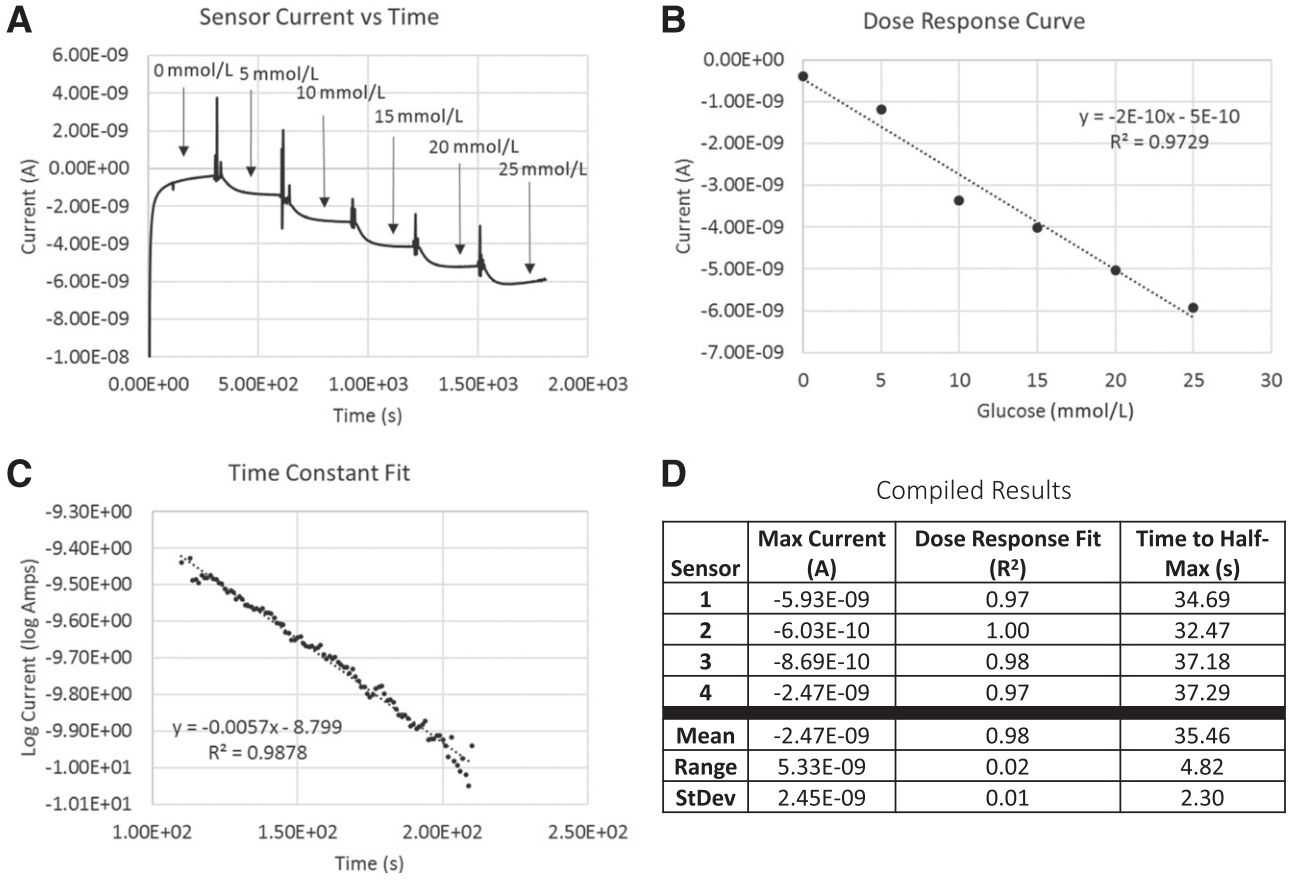

Sensor	Max Current (A)	Dose Response Fit (R^2)	Time to Half-Max (s)
1	-5.93E-09	0.97	34.69
2	-6.03E-10	1.00	32.47
3	-8.69E-10	0.98	37.18
4	-2.47E-09	0.97	37.29
Mean	-2.47E-09	0.98	35.46
Range	5.33E-09	0.02	4.82
StDev	2.45E-09	0.01	2.30

Figure 2— In vitro sensor testing. *A*: Representative plot of raw sensor current vs. time. Current increases in amplitude (i.e., becomes more negative) in response to increasing glucose concentration. When the glucose concentration changes abruptly, the sensor current decays exponentially toward a new steady state. Handling of the sensor between samples caused large, brief deviations in current. *B*: A dose-response curve was generated for each sensor by plotting a 30-s average of sensor current vs. glucose. *C*: The T_{50} sensor response was determined for each glucose value in each sensor by plotting the log of the difference between transient current and steady-state current against time. T_{50} is then calculated from the slope of the resulting line. *D*: Table of results for individual sensors. Amplitude of the glucose response was highly variable, but the dose response was consistently linear, and the T_{50} of the sensor response was consistently ~35 s.

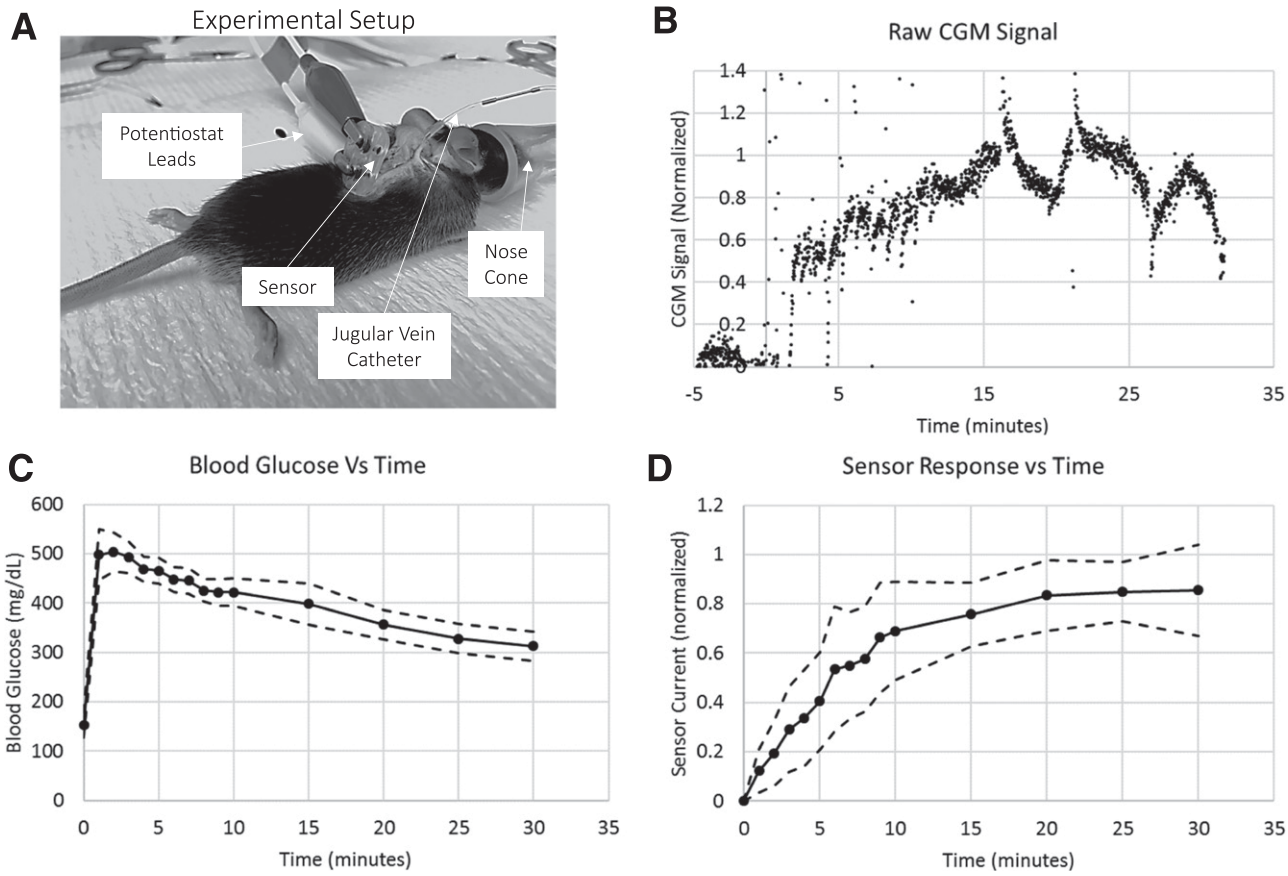

Figure 3—In vivo sensor testing. *A*: Picture of experimental setup. Sensors were implanted below the skin on the mouse's back, and sensor response was recorded after an infusion of dextrose into an indwelling jugular vein catheter. *B*: Example of raw in vivo CGM signal. Noise is substantially greater than in vitro, but electrochemical noise was minor relative to disturbances caused by handling of the mouse while checking blood glucose. *C*: Blood glucose levels peaked within 1–2 min after the intravenous dextrose infusion and then gradually declined for the remainder of the 30-min experiment. *D*: CGM current gradually increased throughout the duration of the experiment, plateauing at ~20 min. Dashed lines in *C* and *D* represent 95% CIs.

but current still increased from baseline in response to increases in blood glucose (Fig. 3*B*). Signal disturbances caused by handling of the mouse when testing blood glucose were large relative to baseline noise. Blood glucose peaked within 2 ± 1 min after the intravenous infusion of dextrose and thereafter gradually declined (Fig. 3*C*, lines represent mean and 95% CIs). In contrast, sensors required 24 ± 7 min to reach maximum current (P = 0.0017) and remained elevated throughout the duration of the experiment (Fig. 3*D*, lines represent mean and 95% CIs). This substantive peak-to-peak delay was produced by a T_{50} of just 7 ± 3 min.

Intravital Microscopy

Intravital microscopy results are summarized in Fig. 4. Representative images of 2-NBDG fluorescence with respect to time are shown in Fig. 4*A*. Fluorescence in the subcutaneous adipose tissue increased rapidly, reaching maximum within 6 ± 6 min (Fig. 4*B*, lines represent mean and 95% CIs). By comparison, fluorescence in the sensor microenvironment increased slowly, requiring 21 ± 7 min to reach maximum (P = 0.0011) (Fig. 4*C*, lines represent mean and 95% CIs). Time to maximum in each tissue exhibited significant variability (e.g., coefficient of variation of 100% in adipose tissue) due to the ambiguity in defining the peak in a long plateau of fluorescence. Assessment of T_{50} was less variable and allowed for direct comparisons to skeletal muscle. T_{50} (Fig. 4*D*) was significantly greater (P = 0.0008) in the sensor microenvironment (3.8 ± 1.8 min) than in non–CGM-implanted subcutaneous adipose tissue (0.8 ± 0.9 min), which in turn was significantly delayed (P < 0.0001) relative to skeletal muscle (1.9 ± 0.5 s).

Histology Results

Histology results are summarized in Fig. 5. The gross morphology of the tissue deposited on CGMs was notably different from adjacent, non–CGM-implanted subcutaneous adipose tissue (Fig. 5*A*). The sensor wire insertion site was visible as a hollow channel through the deposited tissue. Collagen content was assessed using the percentage of total cross-sectional area of the tissue stained positive for Masson trichrome and was significantly increased in sensor deposits (P = 0.0018) (Fig. 5*B*). Collagen content

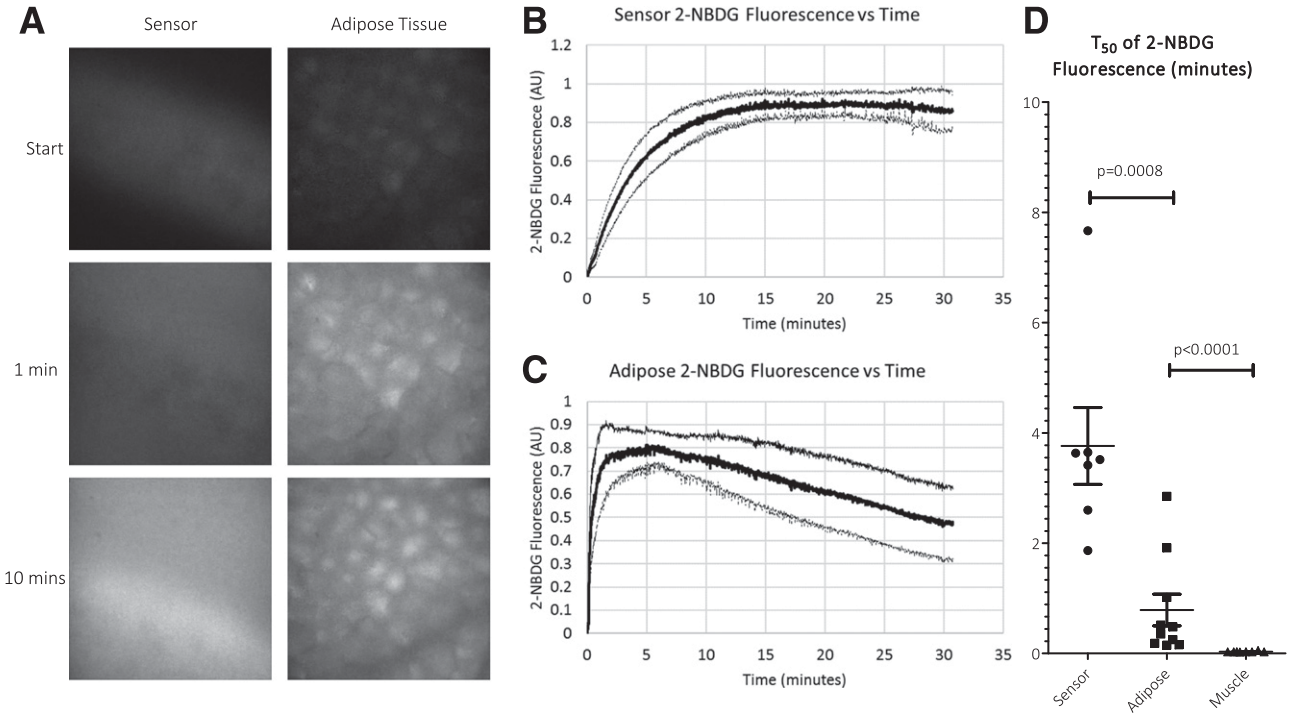

Figure 4—In vivo imaging of 2-NBDG dispersion. *A*: Representative images of 2-NBDG fluorescence in the sensor microenvironment and nonimplanted subcutaneous adipose tissue shows a substantial delay in the dispersion of 2-NBDG to the sensor site. Magnification ×4. *B*: Time course of 2-NBDG fluorescence in the sensor microenvironment shows a gradual increase, followed by a plateau beginning ~15 min postinjection and lasting for the remainder of the experiment. *C*: Time course of 2-NBDG fluorescence in nonimplanted subcutaneous adipose tissue shows a rapid increase postinjection, followed by an ~10-min plateau and then a gradual decline. AU, arbitrary units. *D*: Comparison of T_{50} 2-NBDG fluorescence after injection in the sensor microenvironment, subcutaneous adipose tissue, and skeletal muscle shows statistically significant ($P < 0.05$) differences between each compartment. Error bars represent 95% CIs.

was closely correlated with the T_{50} of 2-NBDG fluorescence in vivo ($R = 0.96$, $P = 0.0004$) (Fig. 5*C*).

Data and Resource Availability

The data sets generated during and/or analyzed during the current study are available from the corresponding author upon reasonable request.

DISCUSSION

This study investigated the dispersion of glucose in the CGM microenvironment and found that fibrotic encapsulation of the implanted sensor is the dominant source of CGM latency in vivo. A time course of the events that must occur for changes in plasma glucose to be reflected in CGM signal is illustrated in Fig. 6. These findings are in direct contrast with the hypothesis that CGMs measure physiological interstitial glucose levels (24) and they cannot be accounted for by algorithmic latency, which was excluded in this study by taking high-frequency current measurements directly from the sensor electrodes. In vivo CGM responses after an acute blood glucose excursion were comparable to the kinetics of 2-NBDG equilibration into the sensor microenvironment (compare Figs. 2*D* and 3*C*), and the observed delay in 2-NBDG dispersion far exceeded time required for 2-NBDG to equilibrate into skeletal muscle or non–CGM-implanted subcutaneous adipose tissue. These results are consistent with previous reports showing that substrate diffusion barriers in foreign body capsules can be predicted from the volume occupied by fibrotic tissue masses (18). In contrast to this previous work, the current study used a commercial CGM with a clinically relevant duration of implantation and a fluorescent contrast agent with maximal biophysical similarity to glucose. In this model system, we observed that the time required for 2-NBDG equilibration was closely correlated to collagen content in tissues excised for histological analysis.

These results support the conclusion of Steil and colleagues (3), whose analyses of CGM latency predicted that CGM glucose exposures lag blood glucose with a time constant of 5–10 min. This estimated delay is comparable to the ~6 min required to reach T_{50} 2-NBDG fluorescence in the current study, thus affirming clinically relevant conditions in the current study and robust analysis assumptions in previous works addressing this topic (3,5,25–28). However, the results of the current study also suggest that the normal physiological latency of glucose dispersion into the interstitial fluid of CGM-accessible tissues is not the primary source of this delay. Considering the relative time required for 2-NBDG equilibration in skeletal muscle, subcutaneous adipose tissue, and the CGM microenvironment we observed (Fig. 4*D*),

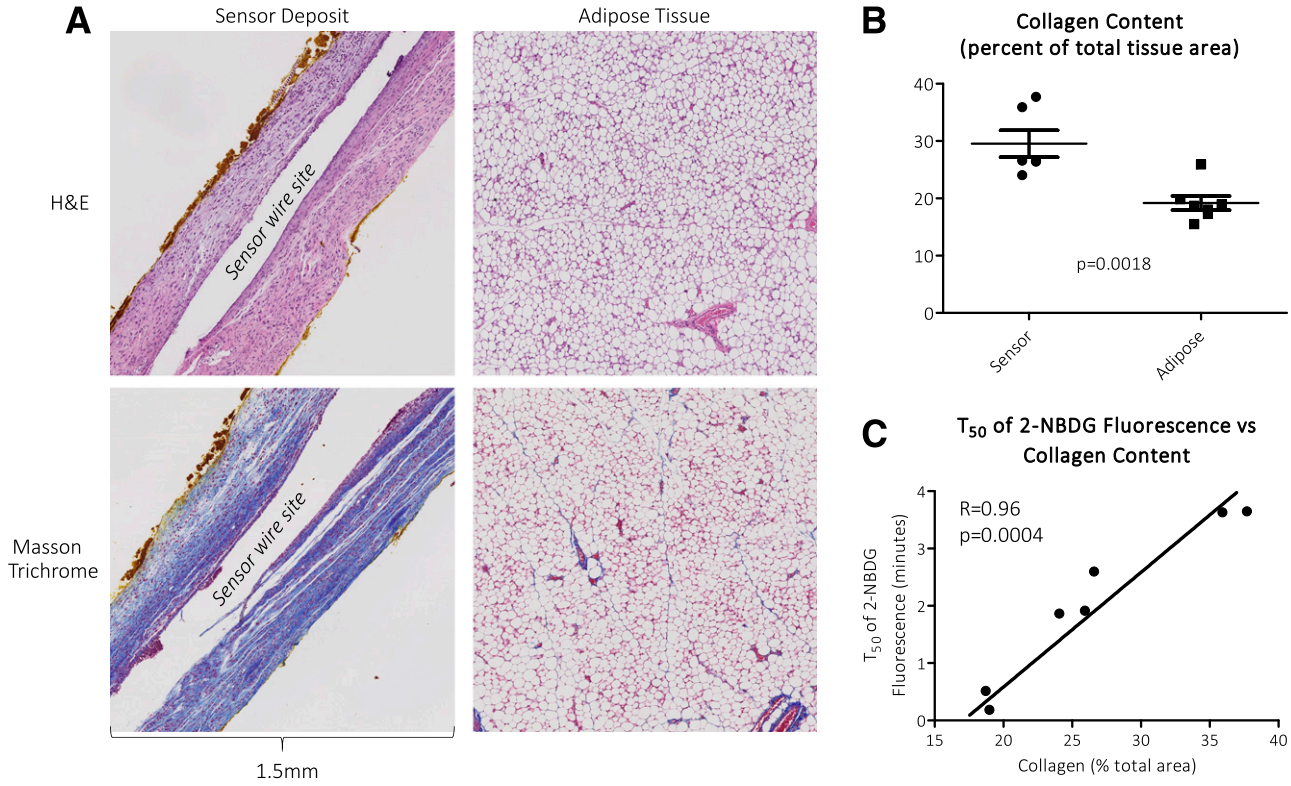

Figure 5—Histological differences between tissue deposited on the sensor and normal subcutaneous adipose tissue. *A*: Representative images of hematoxylin-eosin (H&E) (top) and Masson trichrome (bottom) in tissue deposited on the sensor (left, hollow space left by removal of sensor) and nonimplanted subcutaneous adipose tissue (right). Scale bar applies to both the right and left images. *B*: Collagen content as assessed by percentage of total tissue stained blue by Masson trichrome is significantly greater ($P = 0.0018$) in sensor deposits than in nonimplanted subcutaneous adipose tissue. Error bars represent 95% CIs. *C*: Among samples for which both histology and in vivo 2-NBDG dispersion data were available, collagen deposition was significantly correlated ($R = 0.96$, $P = 0.0004$) with T_{50} 2-NBDG fluorescence.

real-time measurement of interstitial glucose would represent a marked improvement over contemporary CGM technologies. Furthermore, a 5- to 10-min time constant between blood glucose and CGM readings may underestimate the patient-perceived delay (e.g., when monitoring blood glucose for signs of insulin absorption after injection), as evidenced by the ≥20-min peak-to-peak delay in the current study despite a ~7 min T_{50}. The choice to include both T_{50} current and peak-to-peak delay in this report was thus designed to illustrate both the technically well-defined and the clinically relevant delays in CGM readings.

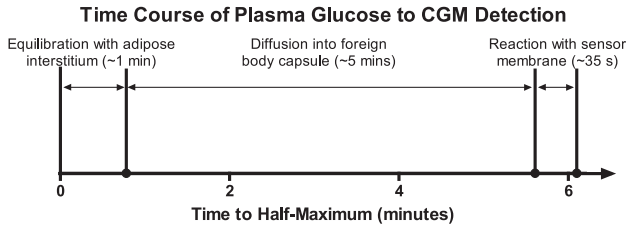

Figure 6—Time course of plasma glucose to CGM detection. Before deviations in circulating glucose can be detected by the CGM, glucose must equilibrate between capillary blood and the adipose interstitium (~1 min to T_{50}), diffuse into the foreign body capsule surrounding the CGM wire (~5 min to T_{50}), and react with the sensor membrane (~35 s to T_{50}). More than 80% of the resulting delay between blood glucose and CGM readings is accounted for by fibrous encapsulation of the implanted CGM.

This distinction between normal interstitial fluid and the CGM microenvironment has several important implications for clinical diabetes research. First, CGMs have occasionally been used as a tool to investigate the kinetics of the interstitial compartment (24,26,27,29), and such studies may substantially understate the rate of glucose exchange between blood and interstitial fluid. This is especially true when using commercially available CGM systems, which include smoothing algorithms to mitigate sensor noise (28). Although it has been suggested that the interstitial fluid sampled by CGMs may better reflect the exposures of key metabolic organs (e.g., brain and muscle) than blood glucose (5), the results of the current study indicate that blood glucose is more representative. Finally, these data show that the theoretical lower bound for CGM latency sensing blood glucose is near-zero. With an intramuscular insertion site, a CGM that evades the foreign body response could plausibly achieve functionally real-time measurements of blood glucose even without algorithms to correct for the time delay.

Realization of this potential would also require strategies to mitigate sensor noise to alleviate the requirement for smoothing algorithms, which can contribute to the

total delay in CGM readings relative to blood glucose (28). Although the current study was not specifically designed to capture these effects, it was visually evident that deviations in sensor current resulting from mechanical disturbances (e.g., moving of the sensor, handling of the mouse, etc.) were very large relative to steady-state sensor noise (see Figs. 1*A* and 2*B*). Considerable progress has been made in the development of algorithms to improve CGM signal processing (30–32), and numerous studies have investigated cellular/biochemical determinants of CGM signal quality (15–17,19,33,34). However, mechanical disturbances seem to have been largely overlooked as a determinant of CGM signal quality. Observations from the current study suggest that the mechanical design of the sensor may be critical for noise mitigation by serving to limit mechanical disturbances at the sensor-electrode and electrode-transmitter interfaces.

These findings also support the premise that fibrosis may hinder glucose diffusion in vivo in other contexts. Extracellular remodeling, including fibrosis and collagen deposition, can occur with insulin resistance in tissues, including skeletal muscle (35), liver (36), and adipose tissue (37). Studies addressing the causality of fibrosis in insulin resistance typically focus on the role of molecular signaling events that govern cellular interactions with the extracellular matrix (38). However, the close association between 2-NBDG latency and collagen content observed in the current study would suggest that collagen deposition may present a biophysical impediment to the dispersion of glucose to insulin-sensitive tissues. Relationships between fibrotic tissue and solute diffusion similar to the current study have been reported (18), suggesting that the association observed in this study is a reproducible consequence of fibrosis.

Although the results of this study are consistent and compelling, it is important to note that the CGM implantation procedure was, by necessity, different in mice than in humans. Likewise, fibrotic responses in mice may differ from those in humans in a strain-dependent manner (39). Any resulting differences in the initial injury response could plausibly influence our results. However, the delays observed in this study are similar to those reported in humans (25), and histological differences in the tissue surrounding an implanted CGM have also been reported in humans (15). Moreover, the C57Bl/J6 mice used for this study exhibit similar foreign body responses to those observed in humans, and results obtained from C57Bl/J6 mice have previously been consistent with those obtained in nonhuman primates (39,40). Finally, fibrosis surrounding implanted CGMs has also been noted in rats, pigs, and dogs (12,41,42) and has been noted as early as 1–3 days after insertion (14,42). Thus, our findings generally recreate results from previous studies, and the novel aspects of this study represent a logical extension of the field.

The CGM itself is located within a surgical wound regardless of implantation technique, and thus the only expected error in our analysis resulting from blunt dissection would therefore be to underestimate glucose equilibration into nonimplanted subcutaneous adipose tissue adjacent to the sensor, which may have experienced excess injury in this study relative to normal CGM implantation procedures. If injury to the surrounding adipose tissue influenced our results, the resulting fibrosis would strengthen the core conclusions of this study, given that the difference between adipose interstitium and CGM microenvironment would thus be even greater without fibrosis in nonimplanted adipose tissue.

An additional consideration is the dynamic processes of tissue remodeling at the sensor insertion site and macrophage recruitment in the first several days after CGM insertion. Newly implanted CGMs are exposed to a complex milieu of blood, interstitial fluid, and infiltrating inflammatory cells. The consequences of these exposures have been carefully addressed by previous works (19). The current study was conducted using time points after the transient period of dynamic healing because the duration of this healing process is short and the response is heterogenous, dependent on the vascularization of the precise site of insertion. The measurement of time lag to the sensor site shortly after insertion will be complicated by these factors. Fibrous encapsulation of implanted CGMs has been demonstrated at 3 days after implantation (14), and thus the foreign body capsule is present during most of a typical 14-day window of implantation using contemporary CGMs (e.g., Dexcom G5, FreeStyle Libre, etc.). Thus, the 7- to 13-day time frame used in the current study was chosen to represent conditions most relevant to most of the lifetime of an implanted CGM.

The key practical implication of these data is that >80% of the latency with respect to blood glucose detection by CGMs is due to fibrous encapsulation of the sensor. Modifications to the CGM membrane that limit foreign body or inflammatory responses, such as a dexamethasone-eluting silicone collar or coating the sensor with a zwitterionic polymer (33,34,43), hold promise not only for their intended purpose of improving signal quality and sensor longevity but also for improving the timeliness of glucose readings. Beyond the CGM field, fibrosis-related impediments to glucose diffusion may also apply to other areas relevant to diabetes and metabolism, including extracellular matrix remodeling in insulin resistance.

Acknowledgments. The authors would like to acknowledge the use of equipment and services provided by the Vanderbilt Nikon Center of Excellence, Mouse Metabolic Phenotyping Center, Translational Pathology Shared Resource, Digital Histology Shared Resource, and Diabetes Research and Training Center.

Funding. This study was funded by National Institutes of Health Clinical Center Grants (DK-059637, DK-054902, DK-050277, T32-DK-101003, DP3-DK-101068, F32-DK-120104, and K12-HD-087023) and the American Heart Association Strategically Focused Research Network at Vanderbilt University.

Duality of Interest. No potential conflicts of interest relevant to this article were reported.

Author Contributions. P.M.M. recognized the discrepancy between clinical and basic science assumptions regarding interstitial glucose latency, designed the study, performed the experiments, and wrote the manuscript. E.S.M. devised the technique for taking high-frequency measurements of sensor current and assisted with both in vivo and in vitro sensor testing. I.M.W. hypothesized that a foreign body response may be a major source of sensor latency, helped to design the experiments, and edited the manuscript. C.M.M. devised the sensor implantation procedure and performed all implantation and catheterization surgeries. F.D.J. assisted in the development of the sensor implantation procedure and logistical arrangements for performing the studies. P.C.L. explained the electrical principles of CGM measurements, helped to devise a method for high-frequency testing, and provided translational insights. J.M.G. provided the sensors used for the study, assisted with the design and interpretation of experiments, and edited the manuscript. D.E.C. provided the potentiostat, explained the chemical principles of CGM measurements, and helped to devise a method for high-frequency testing. D.H.W. recognized the discrepancy between clinical and basic science assumptions regarding interstitial glucose latency, provided funding for the experiments, and edited the manuscript. P.M.M. the guarantor of this work and, as such, had full access to all the data in the study and takes responsibility for the integrity of the data and the accuracy of the data analysis.

Prior Presentation. Parts of this study were presented in abstract form at the 79th Scientific Sessions of the American Diabetes Association, San Francisco, CA, 7–11 June 2019.

References

1. Schmelzeisen-Redeker G, Schoemaker M, Kirchsteiger H, Freckmann G, Heinemann L, Del Re L. Time delay of CGM sensors: relevance, causes, and countermeasures. J Diabetes Sci Technol 2015;9:1006–1015

2. Bergman J, Mellander L, Wang Y, Cans A-S. Co-detection of dopamine and glucose with high temporal resolution. Catalysts 2018;8:34

3. Rebrin K, Sheppard NF, Steil GM. Use of subcutaneous interstitial fluid glucose to estimate blood glucose: revisiting delay and sensor offset. J Diabetes Sci Technol 2010;4:1087–1098

4. Jansson PA, Fowelin J, Smith U, Lönnroth P. Characterization by microdialysis of intracellular glucose level in subcutaneous tissue in humans. Am J Physiol 1988;255:E218–E220

5. Rebrin K, Steil GM. Can interstitial glucose assessment replace blood glucose measurements? Diabetes Technol Ther 2000;2:461–472

6. Yang YJ, Hope ID, Ader M, Bergman RN. Importance of transcapillary insulin transport to dynamics of insulin action after intravenous glucose. Am J Physiol 1994;266:E17–E25

7. Lipman RL, Raskin P, Love T, Triebwasser J, Lecocq FR, Schnure JJ. Glucose intolerance during decreased physical activity in man. Diabetes 1972; 21:101–107

8. Bashkatov AN, Genina EA, Tuchin VV. Measurement of glucose diffusion coefficients in human tissues. In *Handbook of Optical Sensing of Glucose in Biological Fluids and Tissues*. Tuchin VV, Ed. Boca Raton, FL, Taylor & Francis Group LLC, CRC Press, 2009, p. 587–621

9. Sarelius IH, Duling BR. Direct measurement of microvessel hematocrit, red cell flux, velocity, and transit time. Am J Physiol 1982;243:H1018–H1026

10. Pasarica M, Sereda OR, Redman LM, et al. Reduced adipose tissue oxygenation in human obesity: evidence for rarefaction, macrophage chemotaxis, and inflammation without an angiogenic response. Diabetes 2009; 58:718–725

11. Lillioja S, Young AA, Culter CL, et al. Skeletal muscle capillary density and fiber type are possible determinants of in vivo insulin resistance in man. J Clin Invest 1987;80:415–424

12. Ward WK, Troupe JE. Assessment of chronically implanted subcutaneous glucose sensors in dogs: the effect of surrounding fluid masses. ASAIO J 1999;45: 555–561

13. Gifford R. Continuous glucose monitoring: 40 years, what we've learned and what's next. ChemPhysChem 2013;14:2032–2044

14. Henninger N, Woderer S, Kloetzer HM, et al. Tissue response to subcutaneous implantation of glucose-oxidase-based glucose sensors in rats. Biosens Bioelectron 2007;23:26–34

15. Rigla M, Pons B, Rebasa P, et al. Human subcutaneous tissue response to glucose sensors: macrophages accumulation impact on sensor accuracy. Diabetes Technol Ther 2018;20:296–302

16. Novak MT, Yuan F, Reichert WM. Predicting glucose sensor behavior in blood using transport modeling: relative impacts of protein biofouling and cellular metabolic effects. J Diabetes Sci Technol 2013;7:1547–1560

17. Klueh U, Frailey JT, Qiao Y, Antar O, Kreutzer DL. Cell based metabolic barriers to glucose diffusion: macrophages and continuous glucose monitoring. Biomaterials 2014;35:3145–3153

18. Sharkawy AA, Klitzman B, Truskey GA, Reichert WM. Engineering the tissue which encapsulates subcutaneous implants. I. Diffusion properties. J Biomed Mater Res 1997;37:401–412

19. Novak MT, Reichert WM. Modeling the physiological factors affecting glucose sensor function in vivo. J Diabetes Sci Technol 2015;9:993–998

20. Zou C, Wang Y, Shen Z. 2-NBDG as a fluorescent indicator for direct glucose uptake measurement. J Biochem Biophys Methods 2005;64:207–215

21. Boscari F, Galasso S, Facchinetti A, et al. FreeStyle Libre and Dexcom G4 Platinum sensors: accuracy comparisons during two weeks of home use and use during experimentally induced glucose excursions. Nutr Metab Cardiovasc Dis 2018;28:180–186

22. Williams IM, Valenzuela FA, Kahl SD, et al. Insulin exits skeletal muscle capillaries by fluid-phase transport. J Clin Invest 2018;128:699–714

23. McClatchey PM, Mignemi NA, Xu Z, et al. Automated quantification of microvascular perfusion. Microcirculation 2018;25:e12482

24. Cengiz E, Tamborlane WV. A tale of two compartments: interstitial versus blood glucose monitoring. Diabetes Technol Ther 2009;11(Suppl. 1): S11–S16

25. Keenan DB, Mastrototaro JJ, Voskanyan G, Steil GM. Delays in minimally invasive continuous glucose monitoring devices: a review of current technology. J Diabetes Sci Technol 2009;3:1207–1214

26. Rebrin K, Steil GM, van Antwerp WP, Mastrototaro JJ. Subcutaneous glucose predicts plasma glucose independent of insulin: implications for continuous monitoring. Am J Physiol 1999;277:E561–E571

27. Steil GM, Rebrin K, Hariri F, et al. Interstitial fluid glucose dynamics during insulin-induced hypoglycaemia. Diabetologia 2005;48:1833–1840

28. Voskanyan G, Barry Keenan D, Mastrototaro JJ, Steil GM. Putative delays in interstitial fluid (ISF) glucose kinetics can be attributed to the glucose sensing systems used to measure them rather than the delay in ISF glucose itself. J Diabetes Sci Technol 2007;1:639–644

29. Boyne MS, Silver DM, Kaplan J, Saudek CD. Timing of changes in interstitial and venous blood glucose measured with a continuous subcutaneous glucose sensor. Diabetes 2003;52:2790–2794

30. Bequette BW. Continuous glucose monitoring: real-time algorithms for calibration, filtering, and alarms. J Diabetes Sci Technol 2010;4:404–418

31. Kuure-Kinsey M, Palerm CC, Bequette BW. A dual-rate Kalman filter for continuous glucose monitoring. Conf Proc IEEE Eng Med Biol Soc 2006;1:63–66

32. Facchinetti A, Sparacino G, Cobelli C. Online denoising method to handle intraindividual variability of signal-to-noise ratio in continuous glucose monitoring. IEEE Trans Biomed Eng 2011;58:2664–2671

33. Avula M, Jones D, Rao AN, et al. Local release of masitinib alters in vivo implantable continuous glucose sensor performance. Biosens Bioelectron 2016; 77:149–156

34. Xie X, Doloff JC, Yesilyurt V, et al. Reduction of measurement noise in a continuous glucose monitor by coating the sensor with a zwitterionic polymer. Nat Biomed Eng 2018;2:894–906

35. Kang L, Ayala JE, Lee-Young RS, et al. Diet-induced muscle insulin resistance is associated with extracellular matrix remodeling and interaction with integrin $\alpha_2\beta_1$ in mice. Diabetes 2011;60:416–426

36. Angulo P, Alba LM, Petrovic LM, Adams LA, Lindor KD, Jensen MD. Leptin, insulin resistance, and liver fibrosis in human nonalcoholic fatty liver disease. J Hepatol 2004;41:943–949

37. Spencer M, Yao-Borengasser A, Unal R, et al. Adipose tissue macrophages in insulin-resistant subjects are associated with collagen VI and fibrosis and demonstrate alternative activation. Am J Physiol Endocrinol Metab 2010;299: E1016–E1027

38. Williams AS, Kang L, Wasserman DH. The extracellular matrix and insulin resistance. Trends Endocrinol Metab 2015;26:357–366

39. Kolb M, Bonniaud P, Galt T, et al. Differences in the fibrogenic response after transfer of active transforming growth factor-beta1 gene to lungs of "fibrosis-prone" and "fibrosis-resistant" mouse strains. Am J Respir Cell Mol Biol 2002;27:141–150

40. Veiseh O, Doloff JC, Ma M, et al. Size- and shape-dependent foreign body immune response to materials implanted in rodents and non-human primates. Nat Mater 2015;14:643–651

41. Yu B, Wang C, Ju YM, et al. Use of hydrogel coating to improve the performance of implanted glucose sensors. Biosens Bioelectron 2008;23:1278–1284

42. Kvist PH, Bielecki M, Gerstenberg M, et al. Evaluation of subcutaneously-implanted glucose sensors for continuous glucose measurements in hyperglycemic pigs. In Vivo 2006;20:195–203

43. Koh A, Nichols SP, Schoenfisch MH. Glucose sensor membranes for mitigating the foreign body response. J Diabetes Sci Technol 2011;5:1052–1059